This is the peer reviewed version of the following article: L. Zárybnická, Z. Meloun, J. Šafka, V. Truxová, K. Dvořák, J. Machotová, *J. Appl. Polym. Sci.* 2023, 140(35), e54341, which has been published in final form at https://doi.org/10.1002/app.54341. This article may be used for non-commercial purposes in accordance with Wiley Terms and Conditions for Use of Self-Archived Versions. This article may not be enhanced, enriched or otherwise transformed into a derivative work, without express permission from Wiley or by statutory rights under applicable legislation. Copyright notices must not be removed, obscured or modified. The article must be linked to Wiley's version of record on Wiley Online Library and any embedding, framing or otherwise making available the article or pages thereof by third parties from platforms, services and websites other than Wiley Online Library must be prohibited.

3D Printed Heterogeneous Cation Exchange Membrane Processed Using Stereolithography

Lucie Zárybnická[1*], Zbyšek Meloun[2], Jiří Šafka[3], Veronika Truxová[3], Karel Dvořák[1], Jana Machotová[4]

[1]Department of Technical Studies, College of Polytechnics Jihlava, Tolstého 16, 586 01 Jihlava, Czech Republic

[2]MemBrain s.r.o., Pod Vinicí 87, 471 27 Stráž pod Ralskem, Czech Republic

[3]The Institute for Nanomaterials, Advanced Technologies and Innovation, Technical University of Liberec, Studentská 1402/2, 461 17 Liberec, Czech Republic

[4]Institute of Chemistry and Technology of Macromolecular Materials, Faculty of Chemical Technology, University of Pardubice, Studentská 573, 532 10 Pardubice, Czech Republic

[*]Corresponding author: Lucie Zárybnická (email: lucie.zarybnicka@vspj.cz)

Abstract

Membrane chemistry belongs to the field in which 3D printing can advantageously also be used because of enabling the production of prototypes with precisely defined dimensions. The presented work aimed to develop new polymeric compositions for heterogeneous cation exchange membranes manufactured using stereolithography (SLA) from commercially available materials. Three types of photo-curable thermoset resins (acrylic resin and two types of epoxy resins) were used as polymer matrixes in combination with strong acid cation exchange resin powder. The membrane production consisted of several stages, namely mixing the photo-curable resin with finely ground cation exchange resin powder, processing using SLA, and appropriate post-curing using UV light and elevated temperature. The work aimed to monitor the influence of the photo-curable resin type and post-curing on the microstructural,

electrochemical, and mechanical properties of resulting membrane objects. The results revealed that heterogeneous cation exchange membranes could be processed using SLA from the mixture of the acrylic photo-curable resin and cation exchange resin powder (weight ratio of 60/40) without the need for post-curing. These products exhibited high permselectivity (93 %), high ion exchange capacity (2.23 meq·g^{-1}), and sufficiently low electrical resistance (2200 Ω·cm), which predetermines them for efficient electrophoretic separation.

Keywords: 3D printing; Stereolithography; Heterogeneous cation exchange membrane; Thermoset photopolymer resin; Electrochemical properties; Electrophoretic separation

1. Introduction

Stereolithography (SLA) printing is an early and widely used 3D printing process that, in its most common form, works by focusing an ultraviolet (UV) laser on a vat of liquid photopolymer resin [1]. After the irradiation with UV light, the photopolymer cures and forms a single layer of the desired 3D object [2]. Then, the build platform lowers one layer, and a blade recoats the top of the tank with resin [3]. This process is repeated for each designed layer until the 3D object is complete [4].

In membrane technology, 3D printing techniques are a relatively new development direction [5–8]. They offer substantial advantages regarding the desired membrane appearance (dimension, shape, and accuracy of the structure) and material type. Spacers, various types of membranes, evaporators, or meshes have been prepared by means of 3D printing. A thin-film composite membrane from fluorinated diamine incorporated into m-phenylenediamine-based polyamide was prepared for reverse osmosis or nanofiltration process by ink-jet printing [9]. A composite membrane composed of a thin polyethersulfone selective layer deposited onto acrylonitrile-butadiene-styrene support was produced by multi-jet printing and exhibited anti-biofouling

behaviour [5]. Membranes from polymer solutions of polylactic acid, polybenzimidazole, and polyvinyl alcohol were processed by microextrusion 3D printing called solvent cast printing [10]. This approach facilitated the manufacture of mechanically isotropic membranes even in the case of currently unprintable high-performance thermoplastics. Membranes from polysulfone [11] and polyamide 6 [12] were produced using the selective laser sintering method.

One of the problems associated with the 3D printing of polymer membranes lies in the restricted build size of membrane objects compared to conventional large-scale membrane production technologies [8,13]. Another disadvantage may be associated with an inappropriate membrane porosity, which is particularly affected by the resolution of a 3D printer [8,14,15]. In the case of the SLA technique, this problem can be mitigated by printing with a longer curing time, decreasing a layer height, and applying a photopolymer resin with adequate viscosity [16].

Among the various 3D printing processes, the SLA technique, as a light-driven process, offers a high resolution [14]. However, it has been rarely used for producing polymer membranes, most probably because of a narrow choice of photo-curable materials and multi-material integration incapability [8,13,17]. To the best of our knowledge, the research on ion exchange membrane processing using SLA has been focused mainly on printing membrane surface patterns so far [18–20]. Other important parameters related to this issue, namely photopolymer resin viscosity, layer height, duration of UV curing, compatibility of ion exchange polymer and photopolymer resin, and the level of photopolymer resin crosslinking, have not been studied in a complex manner or even solely. Therefore, the broad topic of photo-curable ion exchange membrane manufacture and processing via SLA belongs to active research areas.

In this study, we aimed to produce a heterogenous cation exchange membrane using the SLA technique, comparable to the membranes produced by conventional technologies. We focused on the influence of photo-curable resin type (epoxy, acrylic) and the conditions of the post-

curing process (in terms of the duration of simultaneous UV and thermal curing) on the electrochemical, mechanical, and structural properties of membrane objects.

2. Materials and methods

2.1. Materials and chemicals

ABS-like (epoxy type, Prusa, Czech Republic), Flex resin (epoxy type, Prusa, Czech Republic), and Durable (acrylic type, Formlabs, USA) [21] were used as photo-curable thermoset resins. Cation exchange resin HCR-S/S (marked as "CER") was purchased from Dow Chemical, USA. CER was firstly washed and air-dried using a fluid bed dryer (personal design and construction MemBrain, Czech Republic) at a temperature of 130 °C and secondly milled using a vibrating mill Vibrom 42S (Vibrom, Czech Republic).

2.2. Manufacture of membranes

The particular photo-curable liquid thermoset resin was mixed with CER in a ratio of 60/40 (w/w). The mixture was homogenized using a standard laboratory stirrer at 200 rpm for 5 minutes. For membrane compositions based on ABS-like resin or Flex resin, 3D printing was performed on a 3D printer Prusa SL1 (Prusa, CZE) using a Liquid Crystal Display (LCD) technique generating UV light of the wavelength of 405 nm. For the membrane compositions based on Durable resin, 3D printing was performed on a 3D printer Form 2 (Formlabs, USA). 3D models have been created and edited by SW FreeCad in STereo Lithography format and exported in G-code. The 3D printing parameters are listed in Table 1. Resulting membrane objects in the form of a sheet with dimensions of 40×40×0.4 mm^3 (length, width, height) were washed in isopropyl alcohol using a washing station Form Wash (Formlabs, USA) to remove uncured material adhering to the surface of the objects. One-half of the membrane objects of a specific composition were kept for further testing, and the other half of the membrane objects

were post-cured using a Form Cure unit (Formlabs, USA). The post-curing using 405 nm light proceeded at 60 °C for 30 and 60 min, respectively. Concurrently, reference samples (without CER) were similarly prepared from the particular photo-curable resin. The samples were named **X_y_z**, where **X** is the photo-curable sin type: A, F, and D for ABS-like resin, Flex resin, and Durable resin, respectively, **y** is the amount of CER, and **z** is the post-curing time. A schematic illustration of the production of membrane objects is shown in **Figure 1**.

Table 1 Printing parameters.

Photo-curable resin type	Printer	Layer thickness (mm)	UV light exposure time (s)
ABS-like resin	Prusa SL1	0.05	6
Flex resin	Prusa SL1	0.05	6
Durable resin	Form 2	0.05	*

*Not specified by the manufacturer.

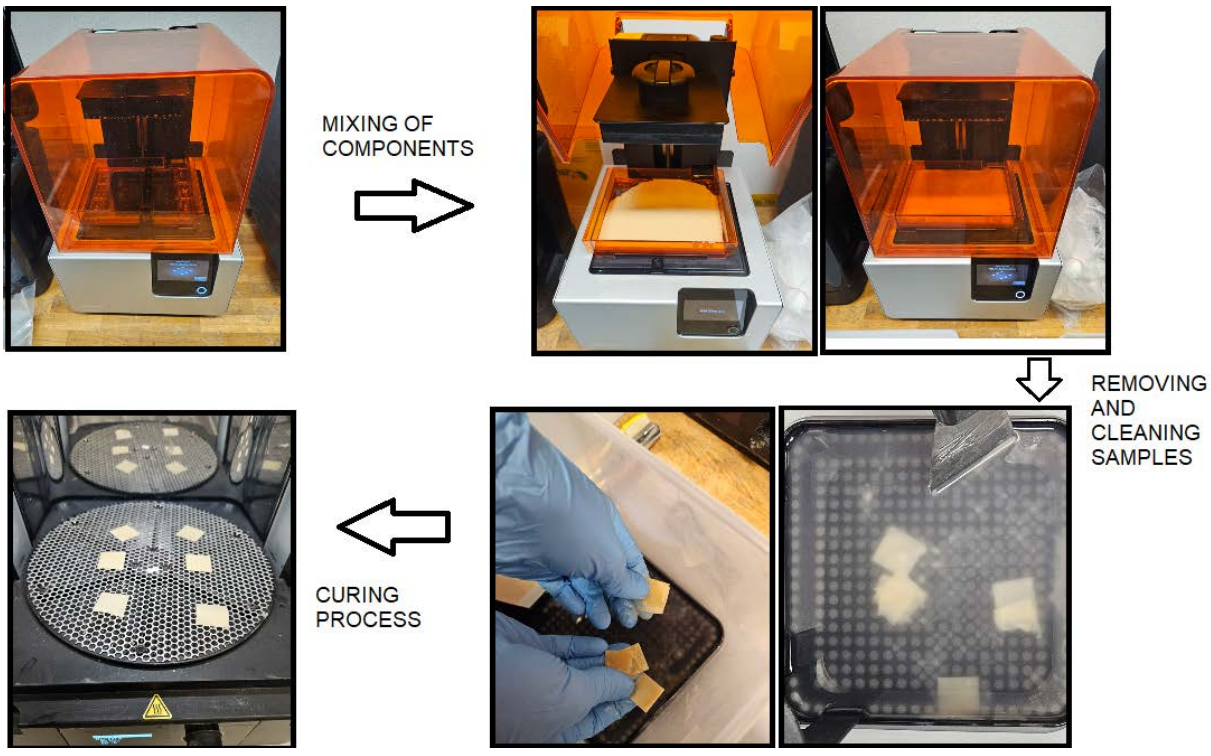

Figure 1 Demonstration of membrane manufacture via SLA.

2.3. Methods

To optimize the CER content in the photo-curable resin mixture, the apparent viscosities[22] of mixtures containing 0–50 wt. % of CER were measured at 25 °C using a Brookfield LVDV-E Viscometer (Brookfield Engineering Laboratories, USA) at 12 rpm according to CSN ISO 2555.

A laser granulometry was used to determine the particle size distribution of CER (DLS Mastersizer 3000E, Malvern) with parameters: refractive index 1.52, density 1 g·cm^{-3}, obscure limit 0.5–8 %, air pressure 2.6 bar, dosing speed 40 %.

SEM Quanta FEG 250 (FEI, USA) and Carl Zeiss ULTRA Plus (Zeiss, Germany) microscopes were used to observe the prepared membrane objects.

The effectivity of the photo-curing process was expressed by crosslink density determined from swelling experiments. Membrane samples (2.0×2.0×0.4 cm^3) were immersed in a solvent (toluene for samples based on Flex resin and Durable resin; isopropyl alcohol for samples based on ABS-like resin) at 25 °C until swelling equilibrium was reached (7 days). After that, the swollen samples were removed, rapidly blotted with wood pulp, and weighed. The average molecular weight between crosslinks (M_c) and the crosslink density (expressed as moles of crosslinks per cm^3 of polymer network) were calculated according to (*Eqs.* 1–4) [23]:

$$M_c = \frac{V_1 \rho_p [\phi^{1/3} - \phi/2]}{-[ln(1-\phi) + \phi + \chi\phi^2]} \quad (Eq.\ 1)$$

$$\phi = \frac{W_p \rho_s}{W_p \rho_s + W_s \rho_p} \quad (Eq.\ 2)$$

$$\chi = 0.34 + \frac{V_1}{RT}(\delta_1 - \delta_2)^2 \quad (Eq.\ 3)$$

$$\text{Crosslink density} = \rho_p / M_c \quad (Eq.\ 4)$$

where V_1 is the molar volume of solvent (76.56, and 106.30 cm^3·mol^{-1} for isopropyl alcohol, and toluene, respectively); ρ_p is the density of the membrane polymer that was calculated based

on the amounts and densities of the individual polymeric components (1.125, 1.07, 1.125, and 1.30 g·cm^{-3} for ABS-like resin, Flex resin, Durable resin, and CER, respectively); φ is the volume fraction of the polymer in the swollen membrane; w_p and w_s are the weight fractions of the polymer and solvent in the swollen membrane sample, respectively; ρ_s is the density of solvent (0.7850, and 0.8669 g·cm^{-3} for isopropyl alcohol, and toluene, respectively); χ is the polymer and solvent interaction parameter; δ_1 is the solubility parameter of membrane polymer that was calculated using the particular ratios and solubility parameters of the individual polymeric components (9.975, 9.385, 9.30, and 9.13 (cal·cm^{-3})$^{1/2}$ for ABS-like resin, Flex resin, Durable resin, and CER, respectively [24,25]); δ_2 is the solubility parameter of solvent (11.6, and 8.9 (cal·cm^{-3})$^{1/2}$ for isopropyl alcohol, and toluene, respectively).

The relative water content was then calculated from the difference in measured weights [26]. The membrane samples were dried in a vacuum dryer at 50 °C to a constant weight. The weighed samples were left in demineralized water to swell for 12 hours. Before weighing, the samples were dried with filter paper to remove the excess water. Relative water content (%) was determined using the relationship (*Eq.* 5):

$$Relative\ water\ content = \frac{m_{wet} - m_{dry}}{m_{dry}}\ x\ 100 \qquad (Eq.\ 5)$$

where m_{wet} is the weight of the sample in the wet form (g); m_{dry} is the weight of the sample in the dry form (g).

For the ion exchange capacity (IEC) measurement, the membrane objects were dried at 105 °C in an oven to constant weight [27]. 50 mL of 0.1 M NaOH was added to 1 g of the dried membrane sample. After 1 h of vigorous stirring, 10 mL of the solution was pipetted, and phenolphthalein was added. The solution was titrated with 0.1 M HCl until the solution discolouration detected the equivalence point. The IEC (meq·g^{-1}) of membrane samples was then calculated according to the relationship (*Eq.* 6) [28]:

$$\mathrm{IEC} = \frac{0.05\left(c_{\mathrm{NaOH}} - \frac{c_{\mathrm{HCl}} V_{\mathrm{HCl}}}{V_{\mathrm{NaOH}}}\right)}{m} \qquad (Eq.\ 6)$$

where V_{HCl} is the volume of HCl solution (mL); c_{HCl} is the exact concentration of HCl solution (mol·L^{-1}); c_{NaOH} is the exact concentration of NaOH solution (mol.L^{-1}); V_{NaOH} is the consumed amount of NaOH solution (mL); m is the weight of dried membrane or granulate sample (g).

Single-parameter basic sensitivity analysis [29] was performed for the IEC determination. The influence of the individual variables used on the IEC results can be seen in Table 2.

Table 2 Single parameter basic sensitivity analysis for *Eq.* 6.

Equation	Parameter	Accuracy	Parameter change by value (%)
6	weight	0.0001 g	0.03 ± 0.00
	volume	0.05 mL	1.25 ± 1.22
	concentration	0.0002 mol·dm^{-3}	0.45 ± 0.44

Determining the electrochemical properties of membrane objects in terms of electrical resistance and permselectivity is important, especially in the case of electrodialysis and electrophoresis separations. The power consumption of the separation process is related to the electrical resistance of a utilized membrane, whereas the effectivity of the separation is associated with membrane permselectivity. The membrane samples (2.0×2.0×0.4 cm^3) were equilibrated in 0.5 M NaCl for 24 hours before the measurement. The electrochemical cell was tempered to 25 °C and the electrical resistance of the samples was measured in a 0.5 M NaCl solution by using a compensation technique. Measurements were carried out in an electrochemical cell, which consisted of two compartments separated by a membrane sample. A defined current of 10 mA was applied to the platinum electrodes and the potential was measured using a couple of calomel electrodes. The specific electrical resistance R_s was determined according to the relationship (*Eq.* 7):

$$R_s = \frac{(U_{\mathrm{IM+sol}} - U_{\mathrm{sol}})}{I} \frac{S}{th} \qquad (Eq.\ 7)$$

where $U_{\mathrm{IM+sol}}$ is the potential of NaCl solution with the embedded membrane sample (V); U_{sol} is the potential of the solution without an inserted membrane sample (V); I is the direct current (10 mA); S is the active area of the membrane sample (0.785 cm^2); th is the thickness of the membrane sample (mm).

The permselectivity P (%) was determined using Henderson's method [26]. The membrane samples (2.0×2.0×0.4 cm^3) were equilibrated in 0.5 M KCl for 24 hours before the measurement. Potentiometric determination of P was carried out in the same electrochemical cell. The separation of KCl solutions of concentrations 0.1 and 0.5 M was performed. Measurements were carried out at room temperature without an applied electric current. Silver chloride electrodes measured the potential generated between the cell compartments. P was subsequently determined according to the relationship (*Eq.* 8):

$$P = \frac{U_{\mathrm{meas}}}{U_{\mathrm{teor}}}\ 100\ (\%) \qquad (Eq.\ 8)$$

where U_{meas} is the measured potential (V) and U_{teor} is the theoretical potential (V) based on the Nernst law expressed by the relationship in (*Eq.* 9), regarding the activity of cations $a_{K1} \cdot a_{K2}$ and anions $a_{A1} \cdot a_{A2}$ in KCl solution of a given concentration present in separate parts of the cell.

$$U_{\mathrm{teor}} = -\frac{\mathrm{R}T}{2\mathrm{F}} \ln \frac{a_{\mathrm{K1}}\, a_{\mathrm{A1}}}{a_{\mathrm{K2}}\, a_{\mathrm{A2}}} \qquad (Eq.\ 9)$$

where R is the universal gas constant (8.3145 $J \cdot mol^{-1} \cdot K^{-1}$); T is the temperature (K); F is the Faraday constant (96 485 $C \cdot mol^{-1}$).

Single parameter basic sensitivity analysis [29] was performed for the determined quantities of R_s, P, and U_{teor}. The influence of the individual variables used on the tested parameters can be seen in Table 3.

Table 3 Single parameter basic sensitivity analysis for *Eqs.* 7–9.

Equation	Parameter	Accuracy	Parameter change by value (%)
7	current	0.12 mA	1.21 ± 0.00
	area	0.004 cm^2	0.59 ± 0.00
	thickness	0.0004 cm	1.36 ± 0.01
	voltage	1.2 mV	1.99 ± 0.05
8	voltage	1.2 mV	3.83 ± 0.01
	U_{teor} from equation (5)	1.68 %	1.71
9	temperature (20 °C) → activity coefficients	tabulated	1.68
	concentration → activity coefficients	tabulated	0.02 ± 0.00

The mechanical properties, specifically the tensile properties of membrane objects, were determined by an Instron 1122 instrument (Instron, USA) at a speed of 50 $mm \cdot min^{-1}$. The tensile stretching was performed in the same direction as the 3D printing orientation of membrane samples (2.0×3.0×0.4 cm^3). The measurements were performed at room temperature (RT, 25±3°C) and relative humidity (RH, 50±10 %) according to ISO 527-3 [30]. Single-parameter basic sensitivity analysis [29] was performed to describe the influence of the individual variables used on the tested parameters (Table 4).

Table 4 Single parameter basic sensitivity analysis.

Parameter	Reference	U*	U_B (%)**
Load cell Instron 1122, 5 kN	2001 N	4.60	0.11
Calliper micrometre 0–25 mm	10 mm	0.02	0.10
Mechanical caliper 0–150 mm, 0,05 mm	23.5 mm	0.05	0.11
Datalogger Comet, −30 to +70 °C, 0 –100 % RH	23.5 °C	0.05	0.11
Datalogger Comet, −30 to +70 °C, 0–100 % RH	68.3 % RH	1.60	1.17

*Measurement uncertainty.

**Measurement uncertainty evaluated by method B is associated with identifiable sources. The square root of the sum of the squares of the uncertainties from individual sources gives the standard uncertainty of method B. Standard uncertainty values obtained by method B do not depend on the number of repeated measurements.

3. Results and discussion

3.1. Characterization of raw materials

The particle size of CER was determined as follows: d_{10} = 3.45 µm, d_{50} = 13.55 µm, and d_{90} = 31.15 µm, a standard particle size distribution of ion exchange resin particles utilized for the preparation of conventional melt-extruded heterogeneous cation exchange membranes [31].

From the point of view of processability, the viscosity of the starting mixtures is a very important parameter [32]. The viscosity of mixtures containing different amounts of CER (0–50 wt. %) is shown in Figure 2. Both Flex resin and Durable resin-based mixtures exhibited a mild increase in viscosity with increasing CER content, whereas the mixtures based on the ABS-like resin were found to be highly viscous in the case of 40 wt. % of CER content and were even unmeasurable at 50 wt. % of CER content. From a processability point of view, there is a risk of poorer processing of highly viscous liquid materials using SLA technologies [33].

On the other hand, the separation efficiency increases with the increasing content of ion exchange resin. Therefore, membrane compositions comprising 40 wt. % of CER were prepared in all further experiments.

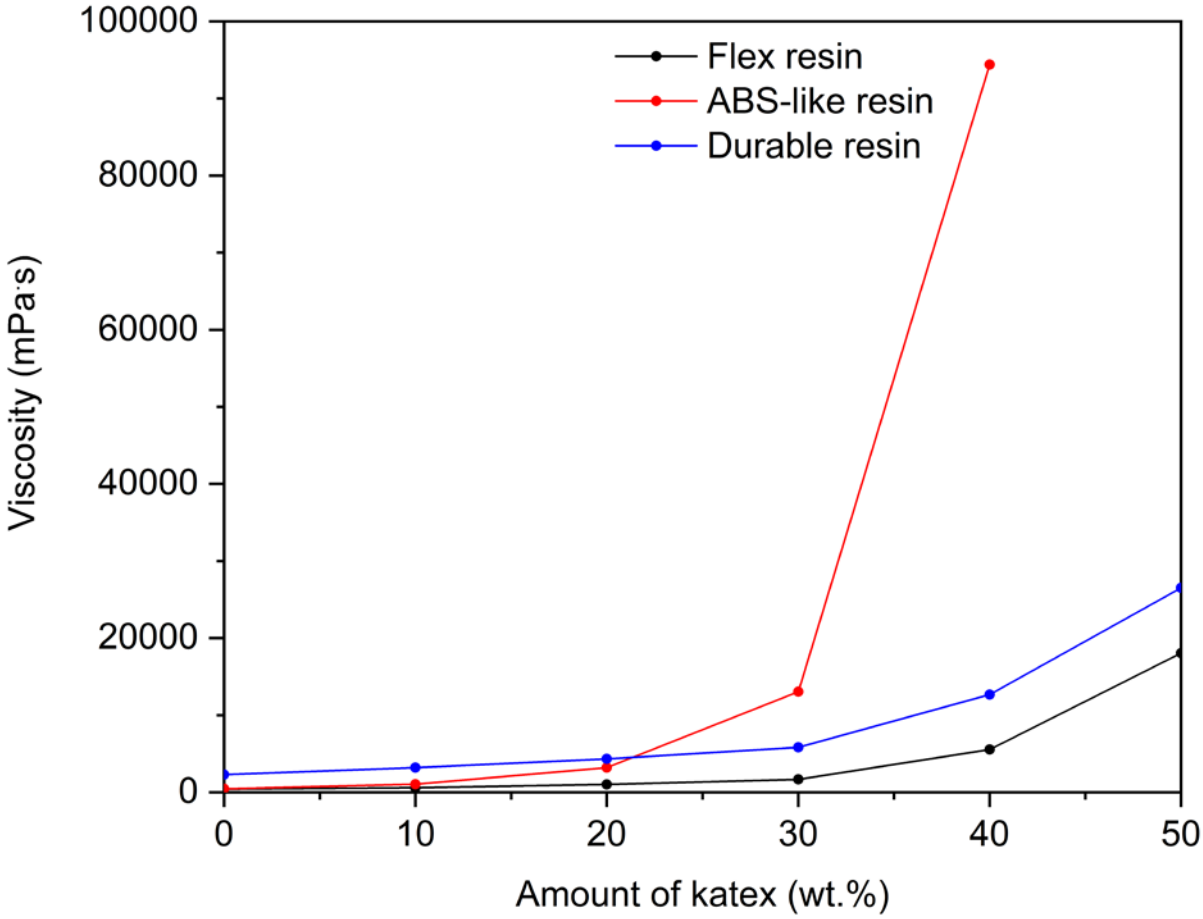

Figure 2 Results of viscosity measurements for mixtures comprising the particular photo-curable resin and CER in different content.

3.2. Characterization of 3D-printed membrane objects

In the case of all membrane objects, the 3D printing was problem-free, there was no clumping of CER particles during printing, and there was no problem with removing the membranes from the 3D printer base. Illustrative photographs of membrane representatives (under normal room conditions) can be seen in Figure 3. The distribution of CER particles in the photopolymer matrix was examined. A homogeneous and regular distribution of ion exchange resin particles in a membrane material predetermines a maximum yield of ion exchange action. SEM pictures (Figure 4) present the cross-section and surface appearance of representative membrane samples. In all cases, CER particles were found to be homogeneously

and regularly distributed in the photopolymer matrix. The surface appearance of membrane samples, especially in the case of A_40_60 and D_40_60, revealed a porous structure, suggesting favorable permeation and transport properties.

On the other hand, the inner structure of the membranes was more compact and did not differ much among the three types of photo-curable polymers. In addition, no significant changes in topography and inner structure of membrane samples were observed in the case of applied post-curing.

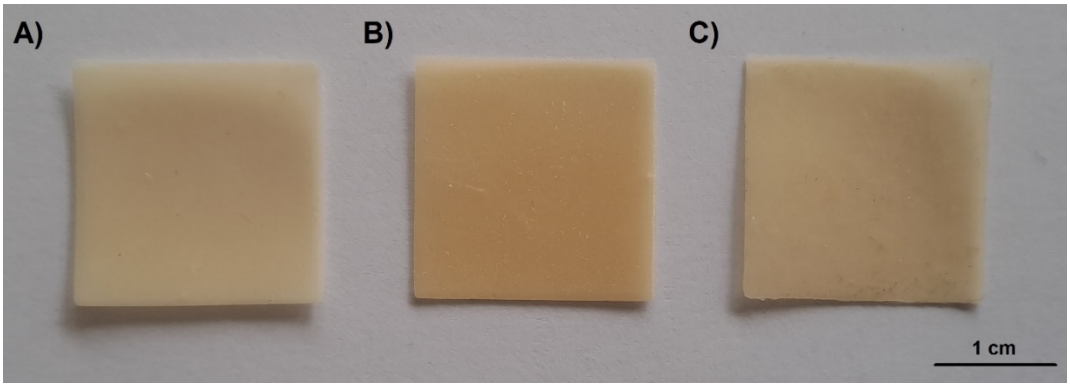

Figure 3 Photographs of membrane samples: A) A_40_60, B) F_40_60, C) D_40_60.

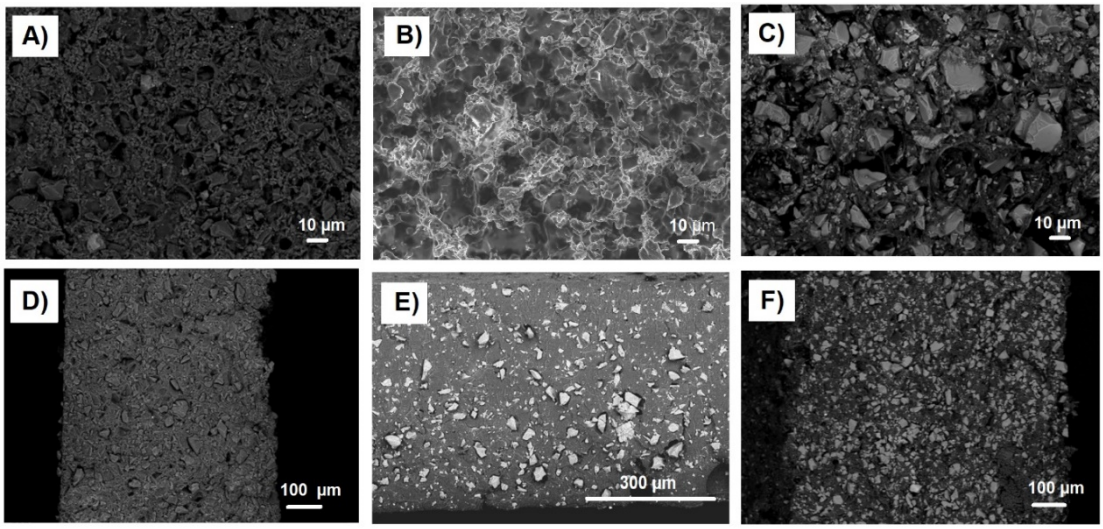

Figure 4 SEM observation of membrane samples: A) A_40_60 surface, B) F_40_60 surface, C) D_40_60 surface, D) A_40_60 cross-section, E) F_40_60 cross-section, F) D_40_60 cross-section.

An important parameter related to appropriately chosen curing parameters within the SLA 3D printing process is the level of crosslinking introduced in the photo-cured polymer matrix [34]. The average molecular weight between crosslinks and crosslink density results are shown in Figure 5. Among the three types of photo-curable resins, the epoxy-based ABS-like polymer matrix showed the highest level of crosslinking, whereas the acrylate-based Durable resin was found to provide the least crosslinked polymer matrix. Membrane samples based on the epoxy-based Flex resin exhibited a comparable crosslinking level, indicating a similar crosslink density of the neat photo-cured matrix and CER polymer (sulfonated styrene-divinylbenzene copolymer gel). Regarding the post-curing, no significant effect was found in the case of all ABS-like and Flex resin-based polymer samples. On the contrary, a significant increase in the crosslink density induced by post-curing was demonstrated in the case of the Durable resin-based photopolymer matrix and membrane samples, where the crosslink density was shown to be enhanced with the duration of post-curing.

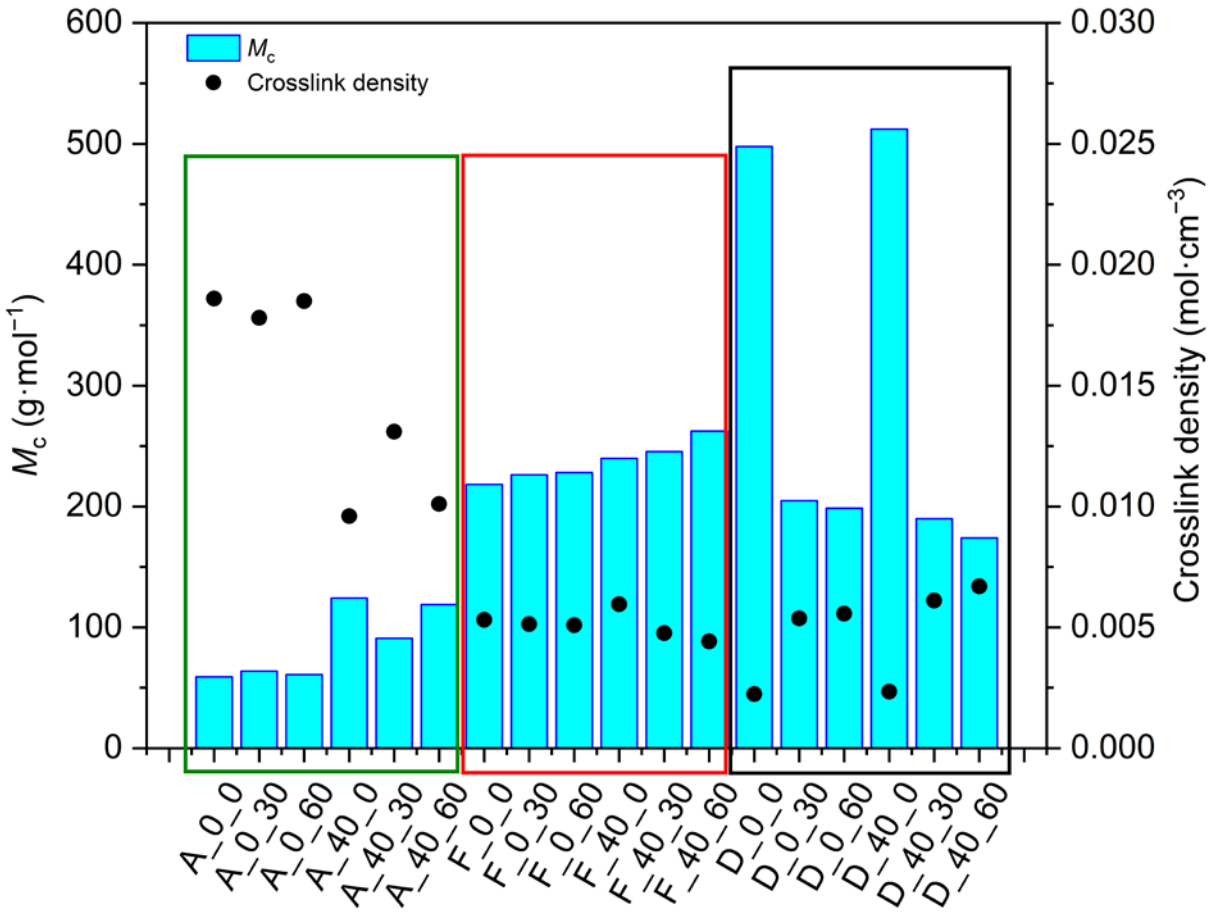

Figure 5 Crosslinking characterization results.

Figures 6 and 7 provide an overview of the electrochemical and separation properties of the prepared membrane samples. *P* is a measure of the ability of a membrane to discriminate between co-ions. If *P* is below 80 %, a high co-ion ratio is transferred through the membrane, considered non-selective and non-separating. The standard *P* value for heterogeneous ion exchange membranes is about 90 %. Another parameter is R_s, representing the resistance of a membrane to electric current, where low R_s indicates a material that readily conducts electric current. The standard R_s values for heterogeneous ion exchange membranes used in electrodialysis [35] and electrophoretic separations are usually lower than 200 and 3000 Ω·cm, respectively. The other important characteristic parameter is IEC, which measures the ability of an ion exchange membrane to undergo displacement of ions previously attached and loosely incorporated into membrane structure by co-ions present in the surrounding solution. Typical

IEC values range between 1.5–3 meq·g^{-1} [36,37]. Among the three types of photo-curable resins, only the membrane samples based on the Durable photopolymer matrix simultaneously showed satisfactory P, R_s and IEC values, indicating their suitability for ion-selective separations. Regarding the post-curing, no significant effect on electrochemical and separation properties was found in the case of all membrane samples.

Electrochemical results are strongly related to the physical changes of membrane objects induced by water swelling, usually represented by the mass change (see Figure 7). An ion exchange membrane must absorb enough water to work properly. On the other hand, it must maintain coherence and consistency in the swollen state. These phenomena are related not only to the type and amount of ion exchange resin but also to the chemical structure and the level of crosslinking of the polymer matrix. A convenient mass change of an ion exchange membrane usually ranges between 45–60% of water, depending on the type of polymer matrix [38]. It was found that all membrane samples exhibited a satisfactory swelling capability between 24–45 % without no significant differences considering photo-curable resin type and post-curing time.

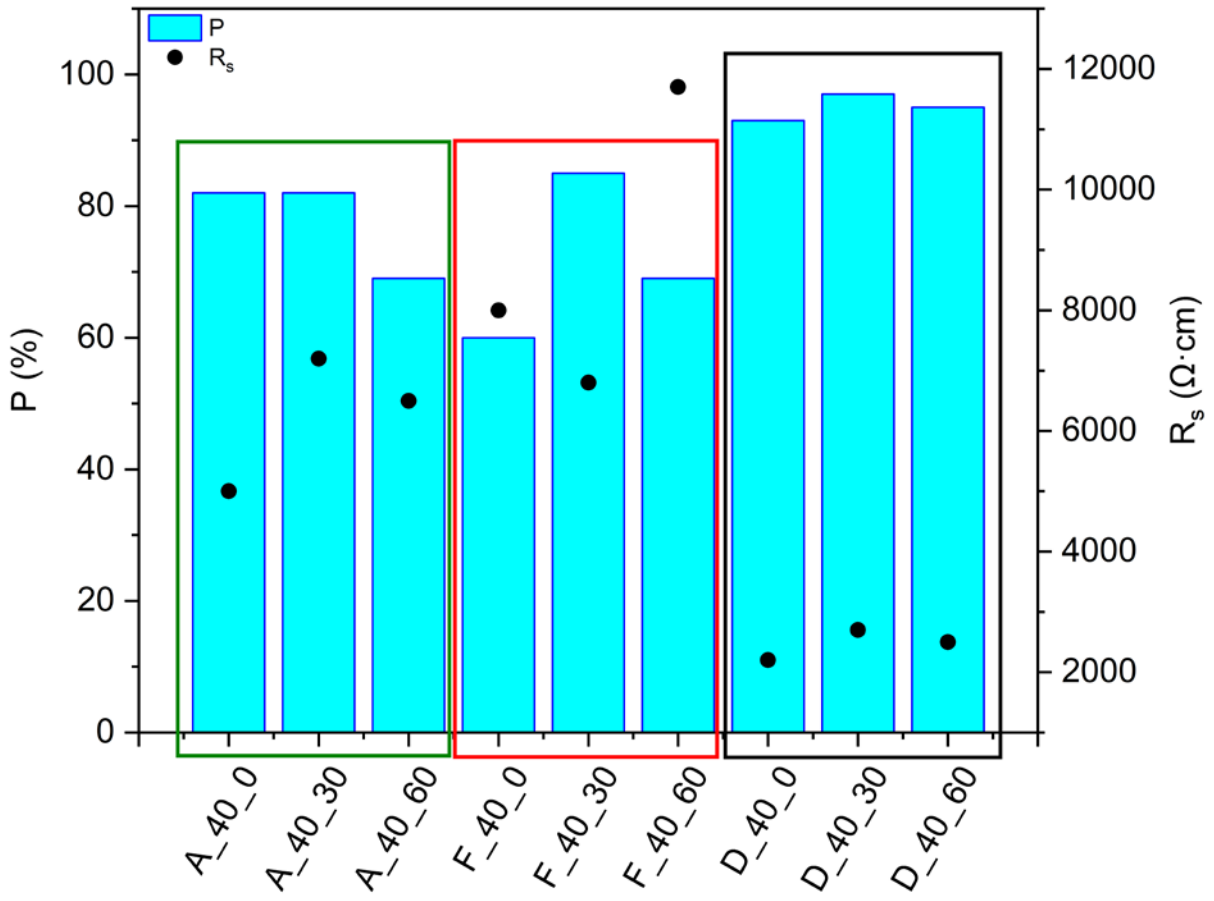

Figure 6 Electrochemical and separation properties of printed membranes.

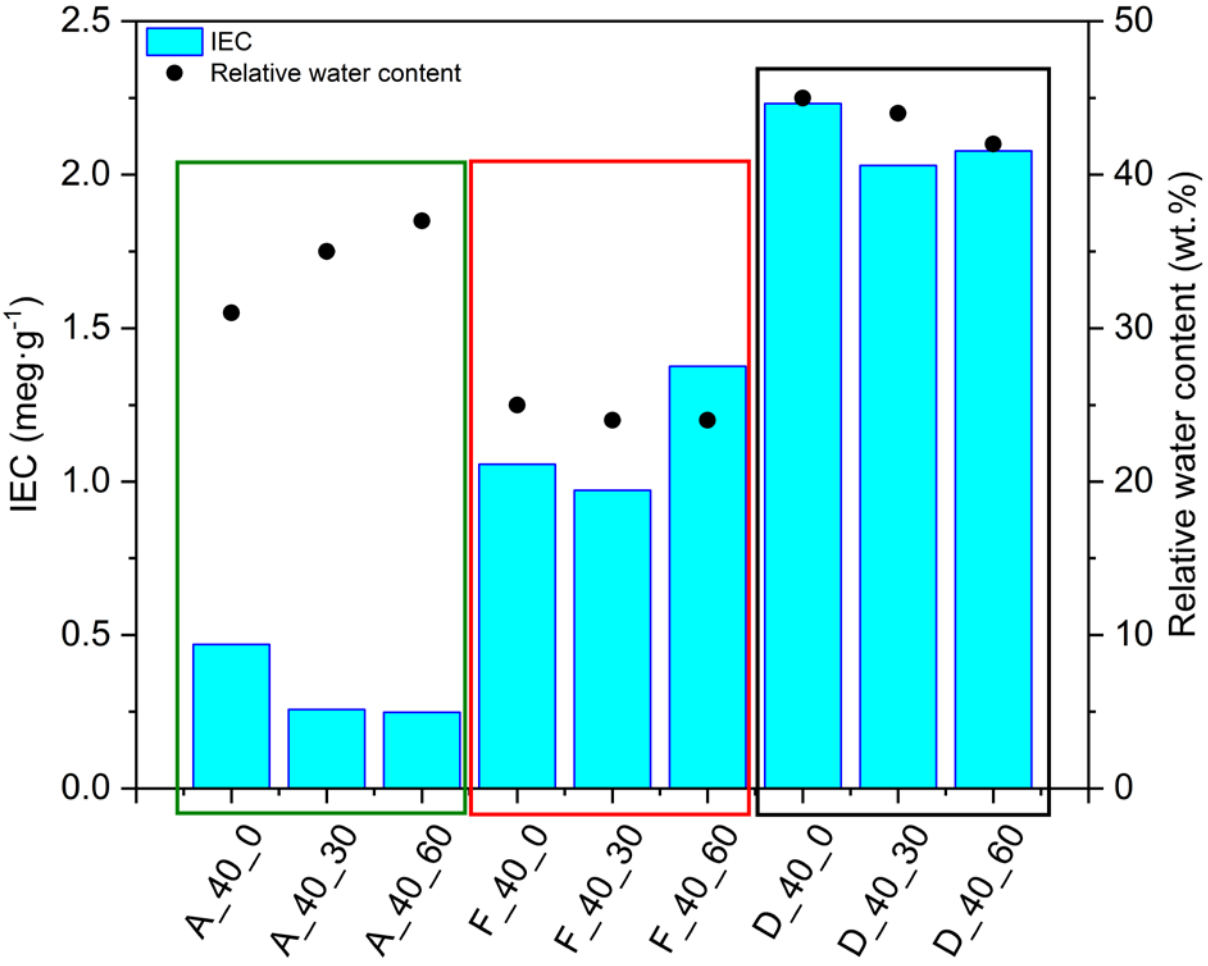

Figure 7 Electrochemical and physical properties of printed membranes.

An important characteristic in the development of ion exchange membranes is also their testing in terms of mechanical properties [39]. The tensile characteristics of neat photopolymer matrixes and membrane samples are shown in Figure 8. Among the three types of neat photopolymer matrixes without the post-curing treatment, the epoxy-based ABS-like polymer showed the highest Young modulus and tensile strength, whereas the epoxy-based Flex resin and the acrylate-based Durable resin were found to provide polymer matrixes with low Young modulus and tensile strength. Focusing on membrane samples without post-curing, the membranes based on Durable resin exhibited the highest values of Young modulus, indicating elasticity and good mechanical resistance. Regarding the post-curing, a pronounced increase in tensile characteristics was found in the case of all neat polymer and membrane samples, whereas the duration of post-curing wasn´t shown to play a significant role. A summary

overview of the results of the electrochemical, physical and mechanical testing is given for clarity in Supplementary Material in Tables S1–S3.

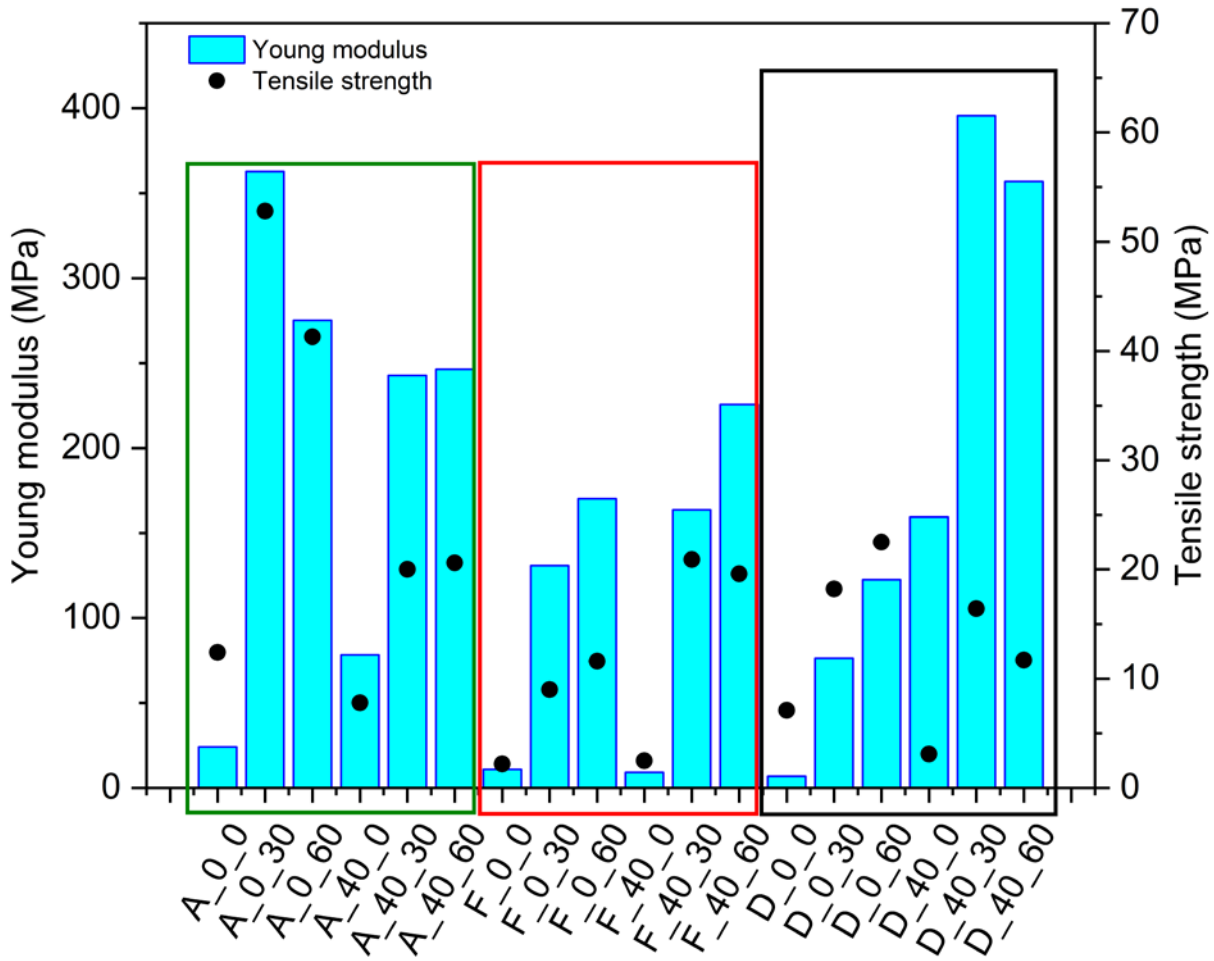

Figure 8 Tensile properties of printed membranes.

4. Conclusion

This work aimed to manufacture 3D-printed heterogeneous cation exchange membranes using stereolithography. Three commercially available photo-curable thermoset resins, namely ABS-like resin (epoxy type), Flex resin (epoxy type), and Durable resin (acrylic type), were tested as polymer matrixes in combination with commercially available cation exchange resin (40 wt. % in the membrane). Concurrently, the influence of post-curing time (using UV light and elevated temperature) on the microstructural, electrochemical, and mechanical properties

of resulting membrane objects was monitored. It was found that only Durable resin provided a convenient photopolymer matrix of 3D printed heterogeneous cation exchange membranes that exhibited high electro-separation efficiency (permselectivity above 93 %, specific electrical resistance in the range of 2200–2700 Ω·cm, and ion exchange capacity above 2.03 meq·g^{-1}), favorable water swelling capacity, and sufficient mechanical properties. Further, post-curing wasn´t proven to significantly enhance the overall performance of the prepared membranes. The developed membranes could find application in electrophoresis, where specific electrical resistance is not the key parameter. Moreover, we aimed to demonstrate that stereolithography is a promising method that offers a targeted preparation of membrane prototypes and membranes which can compete with commercial products produced by conventional large-scale technologies. The advantages of stereolithography for membrane production include: (i) waste-less technology, (ii) precisely defined dimensions of membrane objects, (iii) time and cost savings.

References

1. Savastano, M.; Amendola, C.; Fabrizio, D.; Massaroni, E. In *Digitally supported innovation*; Springer, **2016**; pp 153.
2. Lille, M.; Nurmela, A.; Nordlund, E.; Metsä-Kortelainen, S.; Sozer, N. *J. Food Eng.* **2018**, *220*, 20.
3. Serra, T.; Mateos-Timoneda, M. A.; Planell, J. A.; Navarro, M. *Organogenesis* **2013**, *9*, 239.
4. Zhang, J.; Jung, Y.-G. *Additive manufacturing: materials, processes, quantifications and applications*; Butterworth-Heinemann, **2018**.
5. Al-Shimmery, A.; Mazinani, S.; Ji, J.; Chew, Y. M. J.; Mattia, D. *J. Memb. Sci.* **2019**, *574*, 76.

6. Femmer, T.; Kuehne, A. J. C.; Torres-Rendon, J.; Walther, A.; Wessling, M. *J. Memb. Sci.* **2015**, *478*, 12.

7. Low, Z.-X.; Chua, Y. T.; Ray, B. M.; Mattia, D.; Metcalfe, I. S.; Patterson, D. A. *J. Memb. Sci.* **2017**, *523*, 596.

8. Lee, J.-Y.; Tan, W. S.; An, J.; Chua, C. K.; Tang, C. Y.; Fane, A. G.; Chong, T. H. *J. Memb. Sci.* **2016**, *499*, 480.

9. Badalov, S.; Oren, Y.; Arnusch, C. J. *J. Memb. Sci.* **2015**, *493*, 508.

10. Singh, M.; Haring, A. P.; Tong, Y.; Cesewski, E.; Ball, E.; Jasper, R.; Davis, E. M.; Johnson, B. N. *ACS Appl. Mater. Interfaces* **2019**, *11*, 6652.

11. Yuan, S.; Strobbe, D.; Kruth, J.-P.; Van Puyvelde, P.; Van der Bruggen, B. *J. Mater. Chem. A* **2017**, *5*, 25401.

12. Yuan, S.; Zhu, J.; Li, Y.; Zhao, Y.; Li, J.; Van Puyvelde, P.; Van der Bruggen, B. *J. Mater. Chem. A* **2019**, *7*, 2723.

13. Thiam, B. G.; El Magri, A.; Vanaei, H. R.; Vaudreuil, S. *Polymers (Basel).* **2022**, *14*, 1023.

14. Tan, W. S.; Chua, C. K.; Chong, T. H.; Fane, A. G.; Jia, A. *Virtual Phys. Prototyp.* **2016**, *11*, 151.

15. Qian, X.; Ostwal, M.; Asatekin, A.; Geise, G. M.; Smith, Z. P.; Phillip, W. A.; Lively, R. P.; McCutcheon, J. R. *J. Memb. Sci.* **2022**, *645*, 120041.

16. Hu, Z.; Wang, Y.; Liu, X.; Wang, Q.; Cui, X.; Jin, S.; Yang, B.; Xia, Y.; Huang, S.; Qiang, Z. *Compos. Sci. Technol.* **2022**, *223*, 109403.

17. Yanar, N.; Kallem, P.; Son, M.; Park, H.; Kang, S.; Choi, H. *J. Ind. Eng. Chem.* **2020**, *91*, 1.

18. Capparelli, C.; Fernandez Pulido, C. R.; Wiencek, R. A.; Hickner, M. A. *ACS Appl. Mater. Interfaces* **2018**, *11*, 26298.

19. Seo, J.; Kushner, D. I.; Hickner, M. A. *ACS Appl. Mater. Interfaces* **2016**, *8*, 16656.

20. Muskin, J.; Ragusa, M.; Gelsthorpe, T. *J. Chem. Educ.* **2010**, *87*, 512.

21. X-https://form. x-https://formlabs.com/store/durable-resin/.

22. *ČSN EN ISO 2555 (640346) Plasty - Pryskyřice v kapalném, emulgovaném nebo dispergovaném stavu - Stanovení zdánlivé viskozity použitím rotačního viskozimetru s jednoduchým válcem*; **2019**.

23. Flory, P. J.; Rehner, J. *J. Chem. Phys.* **1943**, *11*, 512.

24. Vandenburg, H. J.; Clifford, A. A.; Bartle, K. D.; Carlson, R. E.; Carroll, J.; Newton, I. D. *Analyst* **1999**, *124*, 1707.

25. Tobing, S. D.; Klein, A. *J. Appl. Polym. Sci.* **2001**, *79*, 2558.

26. Cui, W.; Kerres, J.; Eigenberger, G. *Sep. Purif. Technol.* **1998**, *14*, 145.

27. Zárybnická, L.; STRÁNSKÁ, E.; Machotová, J. In *Waste Forum*; **2017**; Vol. 2017.

28. Zárybnická, L.; Stránská, E.; Večeřa, M.; Černošková, E.; Melánová, K. *Chem. List.* **2015**, *109*, 856.

29. Cacuci, D. G.; Ionescu-Bujor, M.; Navon, I. M. *Sensitivity and uncertainty analysis, volume II: applications to large-scale systems*; CRC press, **2005**; Vol. 2.

30. *ČSN EN ISO 527-3 (640604) Plasty - Stanovení tahových vlastností - Část 3: Zkušební podmínky pro fólie a desky*; **2019**.

31. Stránská, E.; Weinertová, K.; Neděla, D.; Křivčík, J. *Chem. Pap.* **2018**, *72*, 89.

32. Quan, H.; Zhang, T.; Xu, H.; Luo, S.; Nie, J.; Zhu, X. *Bioact. Mater.* **2020**, *5*, 110.

33. Voet, V. S. D.; Strating, T.; Schnelting, G. H. M.; Dijkstra, P.; Tietema, M.; Xu, J.; Woortman, A. J. J.; Loos, K.; Jager, J.; Folkersma, R. *ACS omega* **2018**, *3*, 1403.

34. Sirrine, J. M.; Meenakshisundaram, V.; Moon, N. G.; Scott, P. J.; Mondschein, R. J.; Weiseman, T. F.; Williams, C. B.; Long, T. E. *Polymer (Guildf).* **2018**, *152*, 25.

35. Stránská, E.; Neděla, D. *J. Ind. Text.* **2018**, *48*, 432.

36. Gayathri, R.; Cao, G. *J. Environ. Chem. Eng.* **2022**, *10*, 107025.

37. Cao, G.; Manimuthu, R. P. .

38. Bulejko, P.; Stránská, E. *Mater. Chem. Phys.* **2018**, *205*, 470.

39. Nagarale, R. K.; Gohil, G. S.; Shahi, V. K. *Adv. Colloid Interface Sci.* **2006**, *119*, 97.